Engineering Journal issn: 0125-8281

Article

A Numerical Comparative Study of the Selected Cambered and Reflexed Airfoils in Ground Effect

Mongkol Thianwiboon

Faculty of Engineering, Mahidol University, Nakorn Pathom 73170, Thailand
*E-mail: mongkol.thi@mahidol.ac.th (Corresponding author)

Abstract. When a wing gets closer to the ground, the distortion of the flow and the dynamic air cushion have a positive influence on the aerodynamic characteristics. The vessels that utilize the advantage of this phenomenon in its operation are known as "Wing-in-ground effect craft" or WIG. However, the aerodynamic forces in ground effects are different from free stream flight, especially close to the ground. The center of pressure movement was found to be more complicated and varies with the ground clearance, angle of attack, and the airfoil profile which results in pitching instability in some cases. In this study, a numerical study comparing the aerodynamic characteristics of three commonly used airfoils and one reflexed airfoil in ground effect was carried out with the ground clearance ratio varying from 5% to 100% of the chord at a Reynolds number of 3×10^6 over a wide range of angles of attack from 0° to 20°. As expected, the high-cambered airfoil has the highest lift-to-drag ratio, but the stall occurs at a smaller angle of attack, especially at low ground clearance. It also has a greater center of pressure travel with a strong nose-down moment. The expected reduction of the movement of the center of pressure was obtained in the reflexed airfoil, resulting in better pitching stability at the expense of performance. The performance of the flat-bottom airfoils is compromised between the high-cambered and reflexed airfoil.

Keywords: Wing-in-ground effect craft, WIG, ground effect, airfoil, CFD.

ENGINEERING JOURNAL Volume 27 Issue 11
Received 21 February 2023
Accepted 17 November 2023
Published 30 November 2023
Online at https://engj.org/
DOI:10.4186/ej.2023.27.11.39

DOI:10.4186/ej.2023.27.11.39

1. Introduction

When a fixed wing aircraft flies close to the surface, the air pressure is increased under the wing and leads to the phenomenon known as "ground effect" which increases the lift-to-drag ratio. With lower clearance to the surface, the wingtip vortices and downwash are obstructed by the surface and are difficult to form, which decreases induced drag and increases the lift coefficient. The WIG craft has been developed to take advantage of this phenomenon by flying at low altitude just above the surface with higher speeds than marine vessels and higher efficiency than a conventional airplane [1].

In a free stream flight, NACA6409 is well known as an excellent airfoil for low-speed applications due to it being high cambered [2]. It is believed to be one of the suitable airfoil options for WIG craft which operate at low speed compared to normal aircraft. However, the previous studies of NACA6409 in ground effect by Jung [3], Tahani [4], Jamei [5] indicated that the aerodynamic characteristics in ground effect are different from free stream flight. The flat-bottom airfoils, NACA4412 and Clark-Y, are also widely used due to their simplicity and ease of construction. Many researchers have studied these two flat-bottom airfoils in ground effect experimentally and numerically [6-15].

Previous studies show that during an in-ground-effect flight of a standard airfoil, the aerodynamic forces on the wing cause significant pitching moments, resulting in instability. De-cambering the lower surface and reflexing the trailing edge results in a reflexed airfoil with an 'S' section which can improve stability. The center of pressure (X_{cp}) can be considered stationary within reasonable bounds. This method has the disadvantage of reducing the maximum lift coefficient (C_l) [16, 17]. One of the reflexed airfoils, N60R, which is a modification of the Navy 60 airfoil to obtain a zero-pitching moment for high-speed diving application [18], proved to be more stable. The change in the pitching moment with the clearance between the trailing edge and ground (h) is less noticeable compared to the traditional airfoil and leads to a reduction in the horizontal stabilizer area [12, 19] at the expense of lift.

However, the studies of the airfoils operating in ground effect are still limited to a narrow range of angle of attack (α), typically less than 10°. A direct comparison of the characteristics of the airfoils in ground effect is also missing. The present study is intended to investigate the effects of the camber, the flat shape of the lower surface and the reflexed trailing edge by a direct comparison of the aerodynamic characteristics: lift, drag, pitching moment, and position of the center of pressure. In this study, four airfoils: NACA6409, NACA4412, Clark-Y, and N60R are investigated using the SST k-ω turbulence model. NACA6409 is a high-cambered airfoil; NACA4412 and Clark-Y are flat-bottom airfoils; and N60R is a reflexed airfoil. All investigations were carried out at a Reynolds number (Re) of 3×10^6 based on airfoil chord (c) and h/c ranging from 0.05 to 1 over a wide range of α from 0°-20°. Figure 1 shows these four airfoils relative to the chord line.

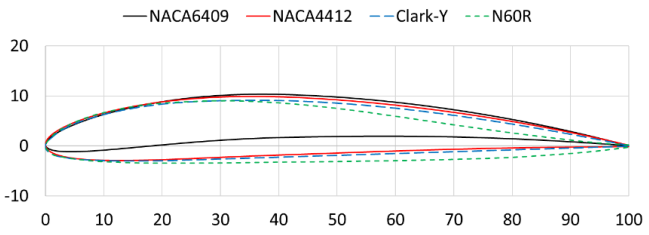

Fig. 1. Geometry of NACA6409, NACA4412, Clark-Y and N60R.

2. Numerical Method and Validation

2.1. Turbulence Model

The numerical investigation of the incompressible flow over the airfoil was carried out by solving the RANS equations with the SST k-ω turbulence model in ANSYS Fluent with a pressure-based double precision solver. A coupled algorithm for the pressure-velocity coupling was selected. The transport equations of the SST k-ω model are described by,

$$\frac{\partial(\rho k)}{\partial t}+\frac{\partial(\rho k u_i)}{\partial x_i}=\frac{\partial}{\partial x_j}\left(\Gamma_k\frac{\partial k}{\partial x_j}\right)+G_k-Y_k+S_k \quad (1)$$

$$\frac{\partial(\rho \omega)}{\partial t}+\frac{\partial(\rho \omega u_i)}{\partial x_j}=\frac{\partial}{\partial x_j}\left(\Gamma_\omega\frac{\partial \omega}{\partial x_j}\right)+G_\omega-Y_\omega+D_\omega+S_\omega \quad (2)$$

G_k, G_ω, Y_k, Y_ω, S_k and S_ω are the generation, dissipation, and user-defined source terms of k and ω respectively. D_ω is the cross-diffusion term. Γ_k and Γ_ω are the diffusivity of k and ω, expressed by,

$$\Gamma_k=\mu+\frac{\mu_t}{\sigma_k} \quad (3)$$

$$\Gamma_\omega=\mu+\frac{\mu_t}{\sigma_\omega} \quad (4)$$

where σ_k and σ_ω are the turbulent Prandtl numbers for k and ω, respectively [20, 21].

2.2. Model Validation in a Free Stream

To validate the accuracy of the numerical method for predicting the flow field and separation, the validation process was performed by computing the flow around a NACA4412 airfoil in a free stream. The process was divided into two stages: 1) performing the grid independence study in a free stream, and 2) comparing the calculated data against the published experimental and numerical data in a free stream.

First, a mesh independence study was carried out, by computing the flow around a NACA4412 airfoil in a free stream with chord length (c) = 1 m. C_l and C_d were determined at Re of 3×10^6 and α = 6°. The density and viscosity of the air were 1.225 kg/m^3 and 1.8375×10^{-5} kg/(m·s), respectively.

DOI:10.4186/ej.2023.27.11.39

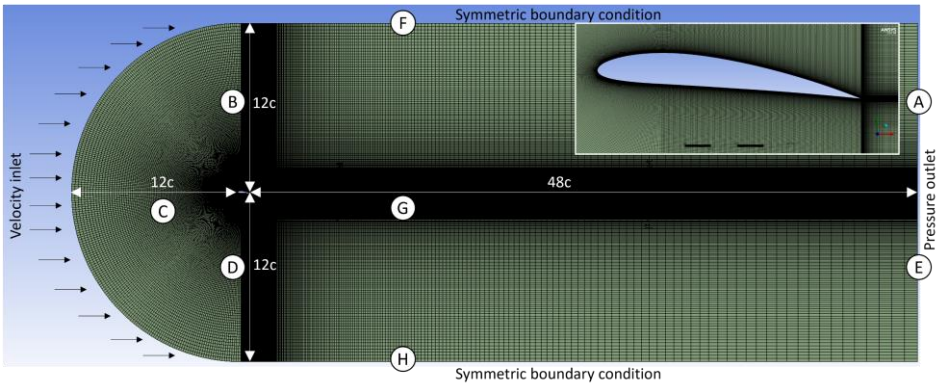

Fig. 2. Generated mesh of the NACA4412 in a free stream at α = 6°.

The computational domain with boundary conditions is shown in Fig. 2. Inlet and outlet boundaries are located 12c and 48c upstream of the leading edge and downstream of the trailing edge, respectively. The distance of 12c from the trailing edge is set to both upper and lower boundaries corresponding to the experimental test section in the variable-density wind tunnel of the National Advisory Committee for Aeronautics [22, 23]. The airfoil surface is set as a non-slip wall. The upper and lower boundary are modeled as a free surface using the symmetric boundary condition. A constant velocity is specified at the inlet boundary and constant pressure is specified at the outlet.

A structured C-type mesh was employed to capture the leading-edge curvature without any singularities. The element size and layer thickness were controlled by the edge sizing parameters to the vertical and horizontal edges, A to H, as shown in Fig. 2. The growth rate of the element was specified with the number of divisions and bias factor on these edges. The relation between the layer thickness (l), edge length (L), number of divisions (n), bias factor (B), and growth rate (G) can be described by:

$$L = l_1 \sum_{i=0}^{n-1} \left(G^i\right) \quad (5)$$

$$B = \frac{l_n}{l_1} = G^{n-1} \quad (6)$$

The first layer non-dimensional height (y+) approximately 1 was specified to resolve the viscous sublayer for the SST k-ω model. The mesh was refined by decreasing the growth rate (G) from 1.2 to 1.02 with ΔG = 0.01 when 1.2 ≥ G ≥ 1.05 and with ΔG = 0.0025 when 1.05 > G ≥ 1.02 until there are no significant changes in C_l and C_d. The results become independent of mesh density at about 250,000 elements (G = 1.04) as shown in Fig. 3.

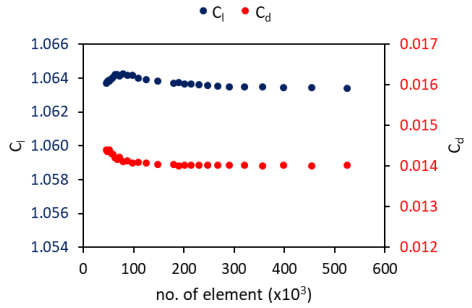

Fig. 3. The mesh independence study result of the NACA4412 in a free stream.

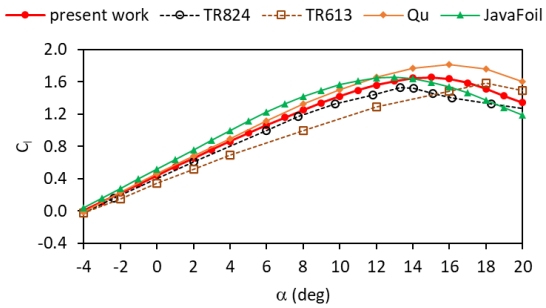

(a) Lift coefficient

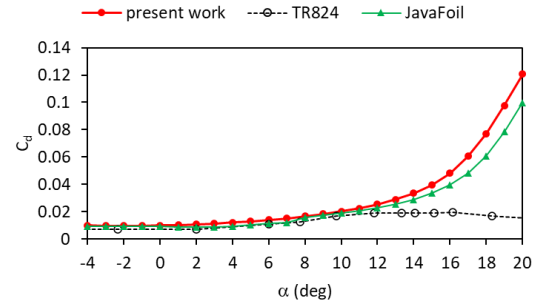

(b) Drag coefficient

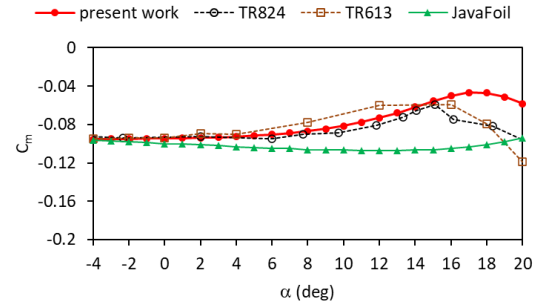

(c) Pitching moment coefficient

Fig. 4. Aerodynamic characteristics of the NACA4412 in a free stream.

After the mesh independence study was carried out, the growth rate (G) of 1.04 was applied to compute the flow around the NACA4412 airfoil in a free stream at Re of 3×10^6 over a range of α from -4° to 20° in the second stage of validation. The present result is validated by comparison with published experimental and numerical data. The sources of experimental data are the NACA Technical reports no.824 and 613 (NACA-TR-824 and 613) [18, 24].

DOI:10.4186/ej.2023.27.11.39

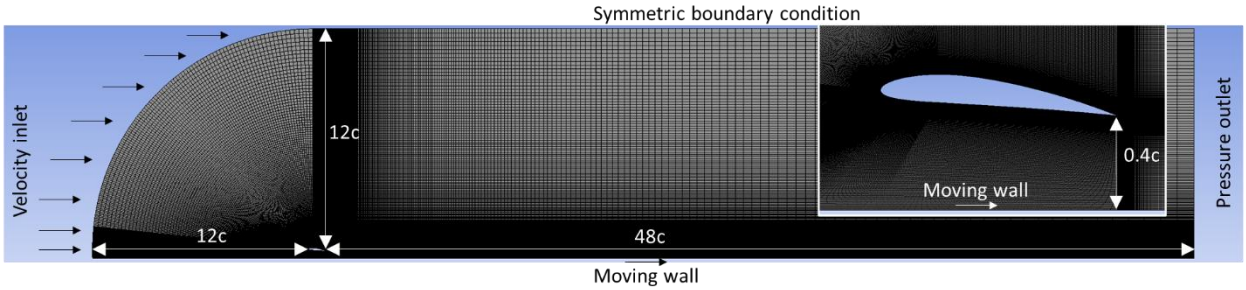

Fig. 5. Computational domain for NACA4412 in ground effect at α = 6° and h_c = 0.4.

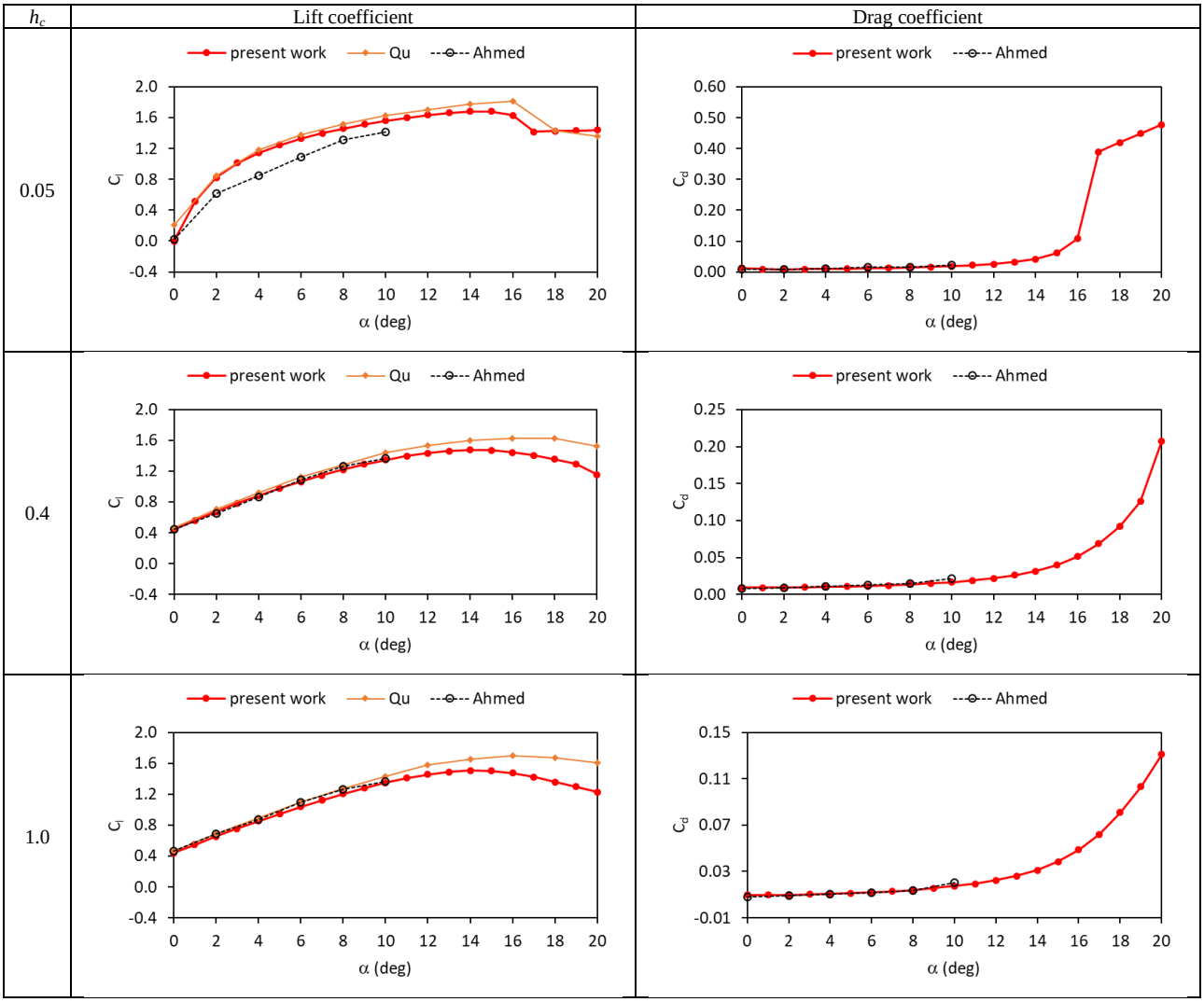

Fig. 6. C_l and C_d of the NACA4412 in ground effect.

The published numerical data is the result from Qu et al. [25]. Additional numerical results were calculated with the JavaFoil algorithm developed by Hepperle [26] based on Richard Eppler's work. [27-29]. Figure 4 shows that C_l of the present work has good agreement with the experimental data, especially NACA-TR-824, at -4° < α < 14° and slightly lower than the result of Qu et al., but close to the numerical data from the JavaFoil. However, due to the fully turbulent flow model of the SST k-ω, the flow separation was delayed [25, 31] leading to over estimation of C_l and C_d, especially at high α.

The prediction of C_m of the present work before stall are accurate compared to the experimental data but slightly higher at high α. The actual unpredicted roughness of the airfoil surface and the difference of Re between the present work and the published data also lead to differences in these coefficients.

2.3. Model validation in ground effect

The flow field and separation of a NACA4412 airfoil in ground effect was computed and validated with the

published numerical and experimental data in the final stage of validation. A structured C-type mesh in Fig. 2 was modified with the distance between the trailing edge and the ground defined as h. The ratio h/c is defined as ground clearance ratio (h_c). The velocity inlet is located $12c$ upstream of the leading edge and the pressure outlet is located $48c$ downstream of the trailing edge. The symmetric boundary condition is set to the upper wall at $12c$ from the trailing edge. The ground is set as a moving wall with the same speed as the inlet velocity. An example of the computational domain is shown in Fig. 5.

The results are validated against the published experimental data from Ahmed et al. [9] and numerical data from Qu et al. [25]. The validation results are shown in Fig. 6.

The figure shows that C_l of the present work has good agreement with both experimental and numerical data at h_c = 0.4 and 1. At h_c = 0.05, C_l deviates slightly from the experiment data but is still close to the numerical data. The C_d prediction is accurate in all cases. Overall, these in-ground-effect validations provide confidence in the ability to predict the aerodynamic characteristics in the ground effect region.

3. Results and Discussion

The method in section 2.2 and 2.3 were used in the numerical investigation of all airfoils, NACA4412, NACA6409, Clark-Y, and N60R, in ground effect with h_c varied from 0.05, 0.1, 0.2, 0.3, 0.4, 0.6, 0.8, and 1. C_l, C_d, C_m and X_{cp} were measured at Re of 3×10^6 and α from 0°-20°.

Ockfen and Matveev [10] reported that both experimental and numerical data are weakly dependent of ground clearance at h_c > 0.36. To represent the pressure coefficient (C_p) and the center of pressure location (X_{cp}) when extremely close to the ground, in transition clearance, and far from the ground effect, h_c of 0.05, 0.3, 0.4, and 1 were selected. The pressure coefficients of the selected airfoils were plotted at α = 6° in Fig. 7. The figure shows that the change in pressure distribution on the upper surface is insignificant with the change of h_c while the pressure on the lower surface is significantly different: lower h_c, the higher C_p, especially at h_c = 0.05. The pressure distribution of N60R significantly differs from the others due to its reversed curvature near the trailing edge, as shown in the pressure contour in Fig. 8.

The comparisons of pressure coefficient distribution between the selected airfoils are shown in Fig. 9. The high camber, NACA6409, produces relatively constant negative pressures on the upper surface over the first 30% from the leading edge. The flat-bottom and reflexed airfoils do not exhibit this behavior. However, it appears that the significant variation of C_p between h_c of 0.3 and 0.4 cannot be detected.

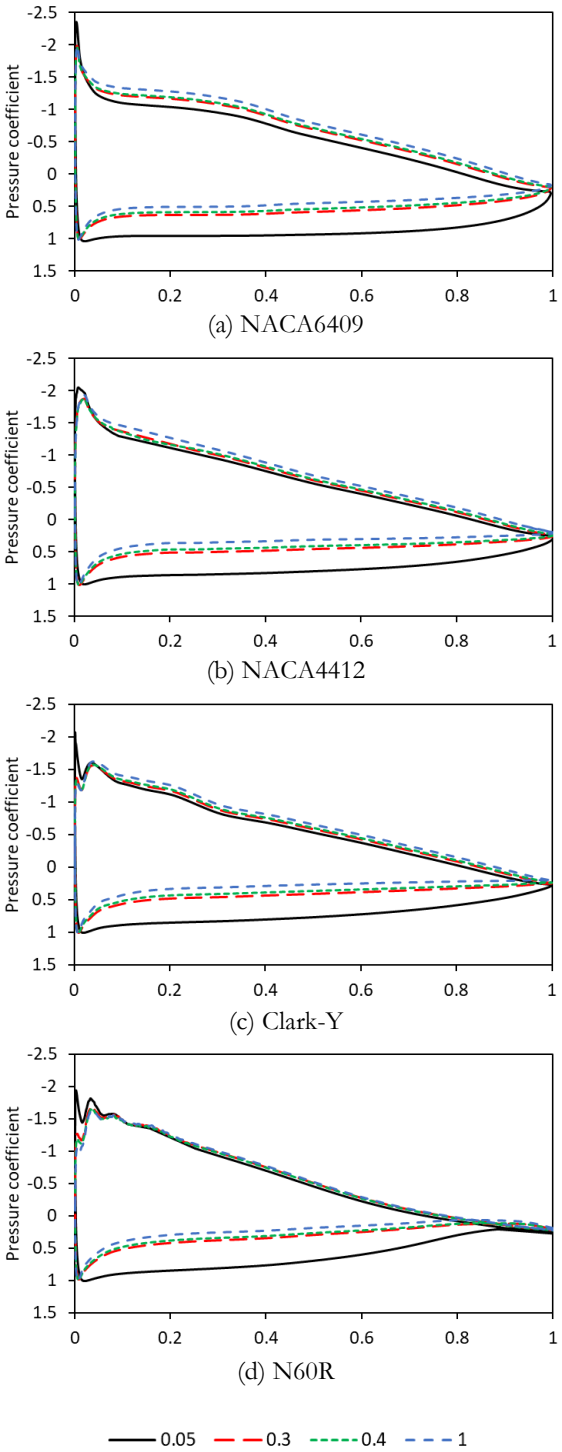

Fig. 7. Pressure coefficient distribution at α = 6°, h_c = 0.05, 0.3, 0.4, and 1.

The lower surface of NACA6409, NACA4412 and Clark-Y experience relatively constant pressure over 80% of the chord while the pressure under the reflexed airfoil, N60R, gradually decreases towards the trailing edge. Thus, the location of X_{cp} of N60R is relatively close to the leading edge compared to the others, as shown in Fig. 10.

DOI:10.4186/ej.2023.27.11.39

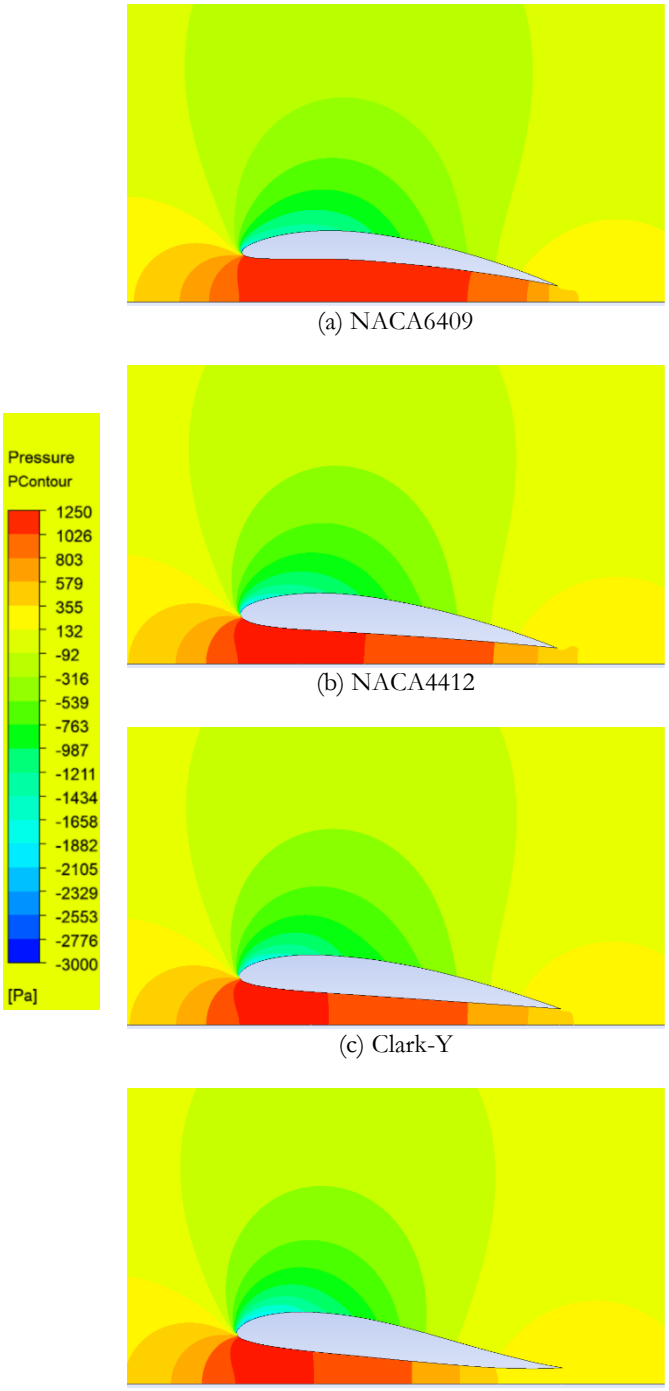

(a) NACA6409

(b) NACA4412

(c) Clark-Y

(d) N60R

Fig. 8. Pressure contour at $\alpha = 6°$, $h_c = 0.05$.

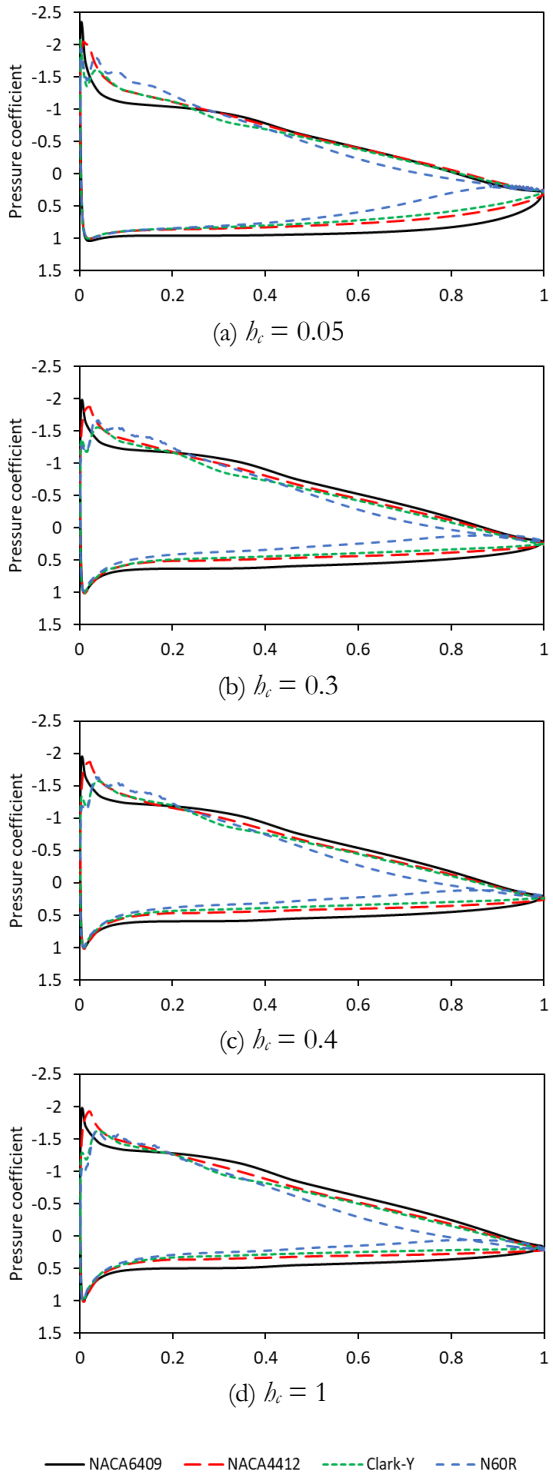

(a) $h_c = 0.05$

(b) $h_c = 0.3$

(c) $h_c = 0.4$

(d) $h_c = 1$

Fig. 9. Comparison of pressure coefficient distribution at $\alpha = 6°$, $h_c = 0.05$, 0.3, 0.4, and 1.

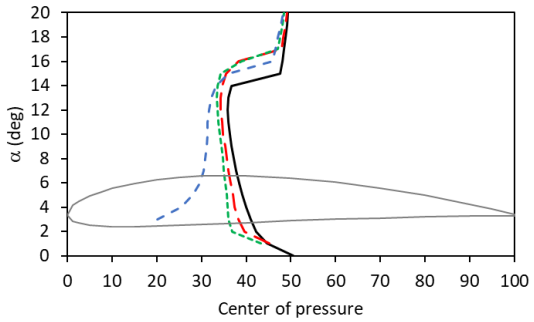

(a) h_c = 0.05

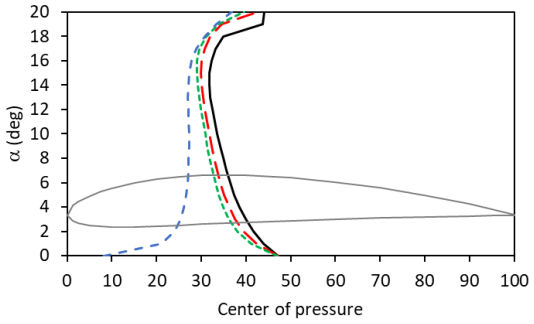

(b) h_c = 0.3

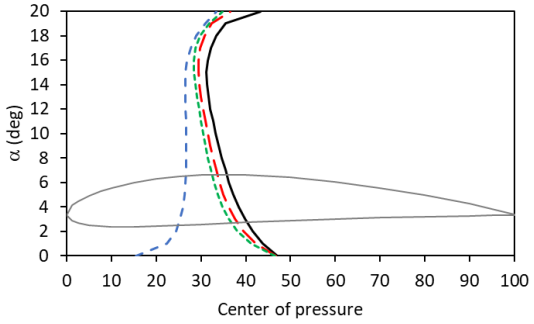

(c) h_c = 0.4

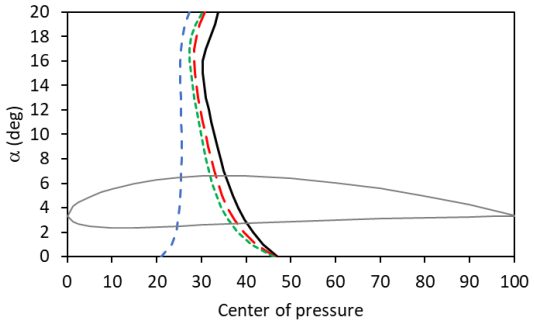

(d) h_c = 1

Fig. 10. Comparison of X_{cp} between selected airfoils at h_c = 0.05, 0.3, 0.4, and 1.

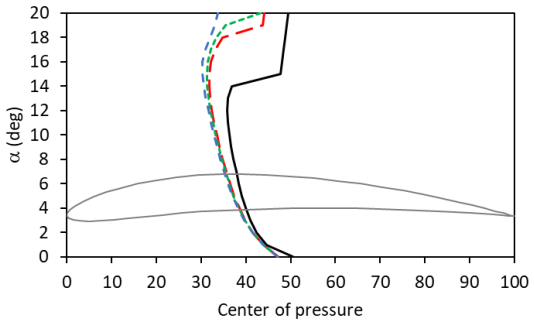

(a) NACA6409

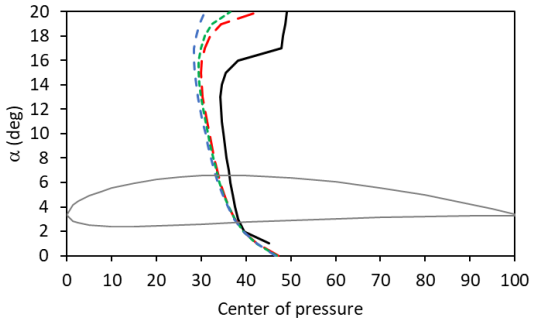

(b) NACA4412

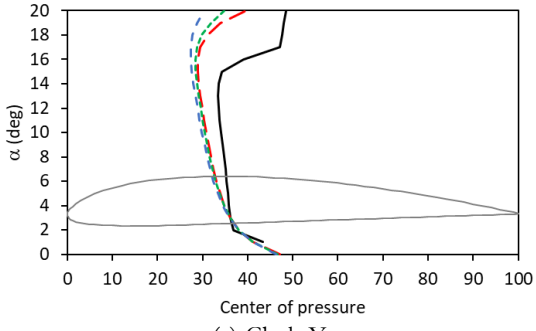

(c) Clark-Y

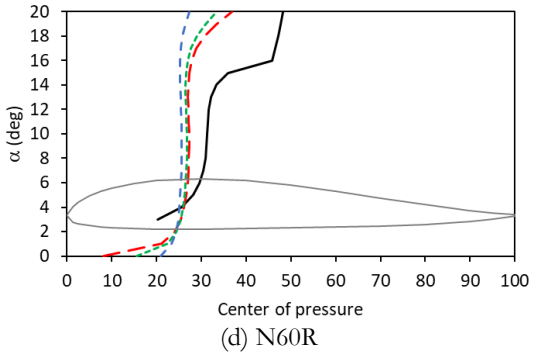

(d) N60R

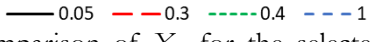

Fig. 11. Comparison of X_{cp} for the selected airfoils at various h_c.

The reflexed airfoil also has less movement of X_{cp} due to less pressure on the lower surface and less negative pressure on the upper surface at the expense of lift. X_{cp} of NACA6409, NACA4412 and Clark-Y gradually moves aft as α decreases and significant shifting rearward of X_{cp} from ~40%c to ~50%c is obviously detected at high α. Lower h_c produces earlier rearward movement of X_{cp} at high α, especially in a high-cambered airfoil.

This causes a nose-down pitching moment that must be counteracted by negative lift in the horizontal stabilizer, as shown in Fig.11. On the other hand, the airfoil exhibits a pitch up tendency when ascending out of the ground effect and becomes unstable.

The pitching moment coefficients of NACA6409, NACA4412 and Clark-Y at various h_c over a range of α and its derivative, $\partial C_m/\partial h_c$, are shown in Fig.12 and 13. It is clearly seen that the pitching moment coefficients are relatively constant for $h_c > 0.4$ but increase slightly ($\partial C_m/\partial h_c > 0$) at $h_c \leq 0.4$.

DOI:10.4186/ej.2023.27.11.39

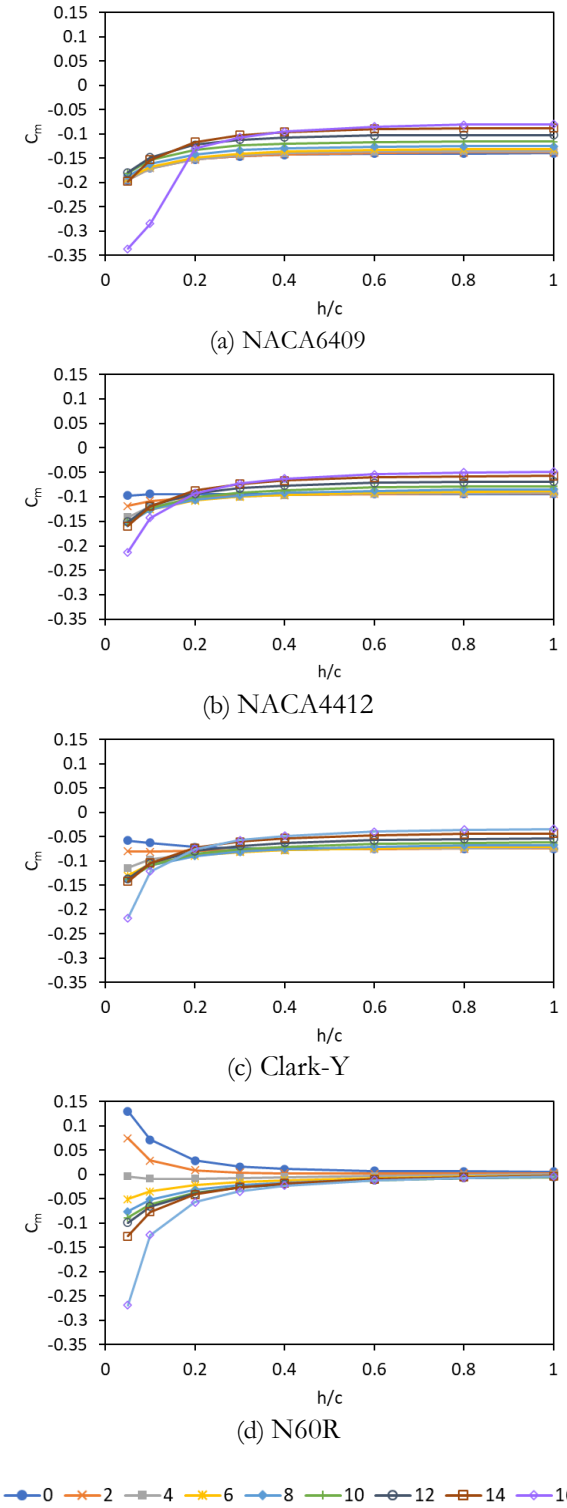

Fig. 12. Pitching moment coefficient versus h_c over a range of α.

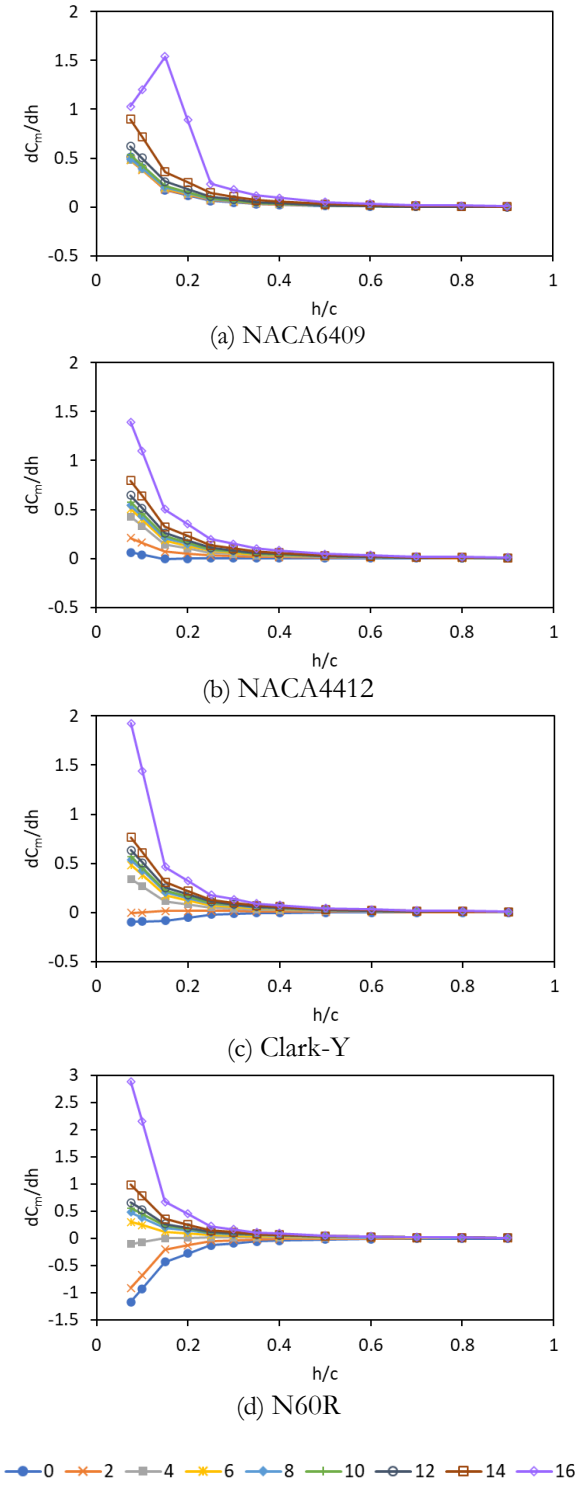

Fig. 13. Comparison of $\partial C_m/\partial h_c$ over a range of α.

This agreed with the published experimental and numerical data [10-15]. However, C_m of N60R is close to zero and does not change significantly with the exception at low ground clearance ($h_c \leq 0.4$) where C_m increases at $\alpha \geq 6°$, but a nose-down moment occurs at $\alpha < 6°$. The comparisons of the C_m at its derivative, $\partial C_m/\partial\alpha$, at h_c = 0.05, 0.3, 0.4, and 1 are shown in Fig .14 and 15. The strong increase in nose-down moment occurs at lower α, especially in a high-cambered airfoil, at extremely low h_c.

For static stability, the derivative of $\partial C_m/\partial h_c$ and $\partial C_m/\partial\alpha$ should be negative [13, 31]. NACA6409, NACA4412 and Clark-Y are unstable in ground effect since these derivatives are positive, as shown in Fig. 13 and 15 while the derivatives of N60R are negative and the airfoil is stable in a restricted zone of operation.

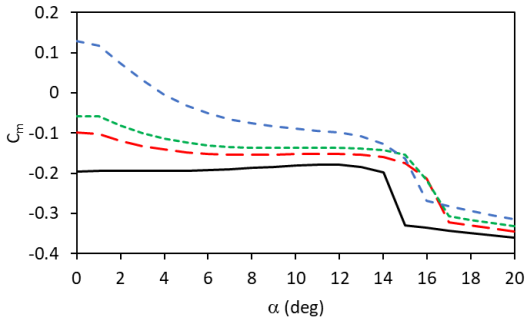

(a) $h_c = 0.05$

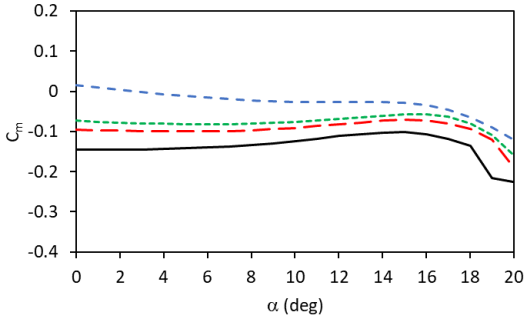

(b) $h_c = 0.3$

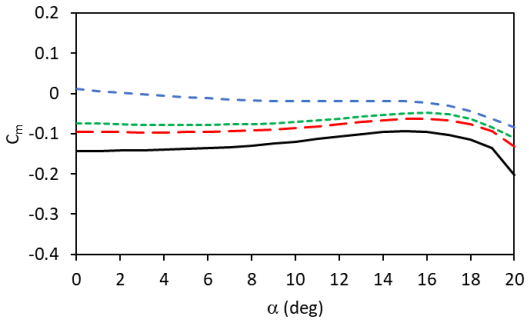

(c) $h_c = 0.4$

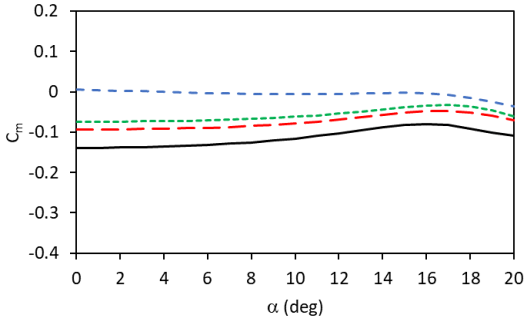

(d) $h_c = 1$

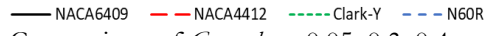

Fig. 14. Comparison of C_m at h_c = 0.05, 0.3, 0.4, and 1.

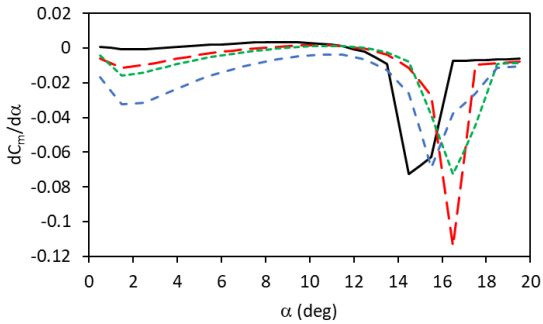

(a) $h_c = 0.05$

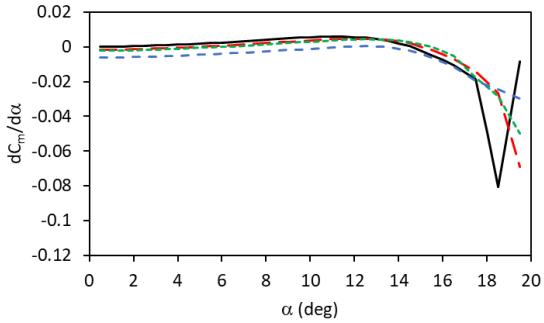

(b) $h_c = 0.3$

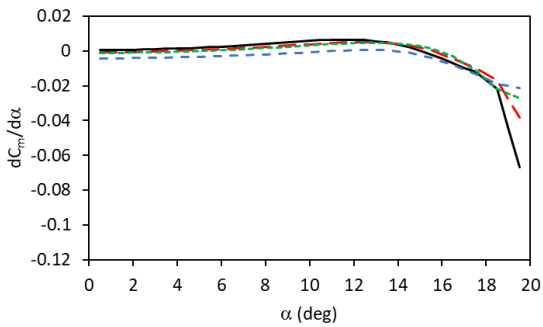

(c) $h_c = 0.4$

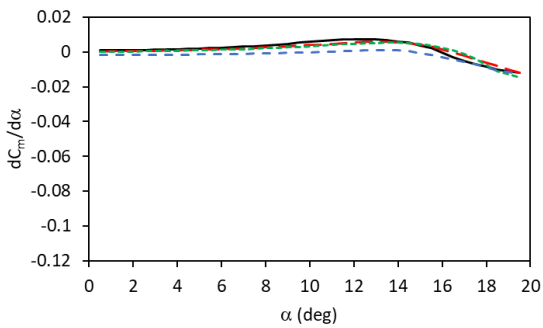

(d) $h_c = 1$

Fig. 15. Comparison of $\partial C_m/\partial\alpha$ at h_c = 0.05, 0.3, 0.4, and 1.

The lift and drag coefficients of the selected airfoils plotted against α are shown in Fig. 16 and 17, respectively. The NACA6409 has the highest lift. NACA4412 and Clark-Y lift curves are almost identical while N60R lift is the lowest. For $h_c \geq 0.4$, a linear portion of the lift curve occurred before stall. The lift curve slope of approximately 5 per radian is relatively constant up to α of 8° for NACA6409, 5.5 per radian for NACA4412 and Clark-Y, and 6 per radian for N60R. The lift curve exhibits greater curvature at lower h_c.

The maximum C_l occurs at α approximately 14° for all h_c. At h_c = 0.05, the maximum C_l of NACA4412, Clark-Y are almost identical to NACA6409, but the maximum C_l of N60R is approximately 7.1% lower. At h_c = 0.3, the maximum C_l of NACA4412, Clark-Y and N60R is approximately 3.3%, 3.9% and 11.8% lower than NACA6409, respectively. Differences become 4.4%, 6.3% and 15.2% lower than NACA6409 at h_c = 1.

DOI:10.4186/ej.2023.27.11.39

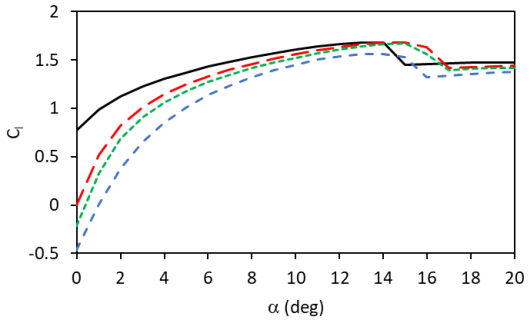

(a) $h_c = 0.05$

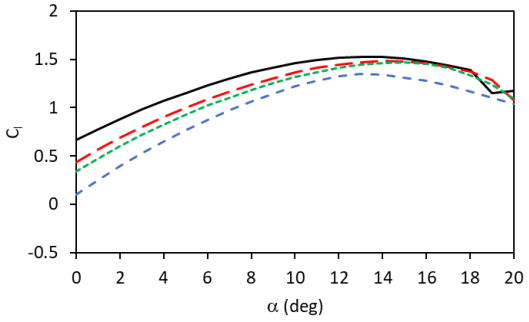

(b) $h_c = 0.3$

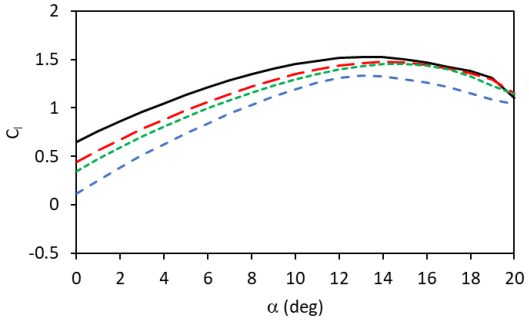

(c) $h_c = 0.4$

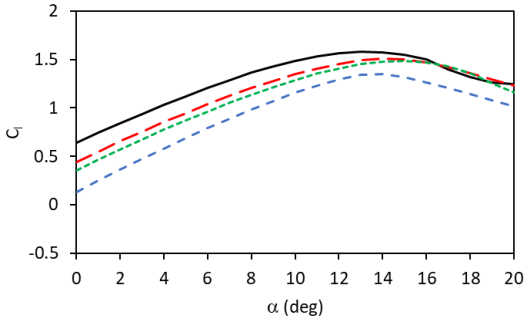

(d) $h_c = 1$

Fig. 16. Lift coefficient for different angles of attack.

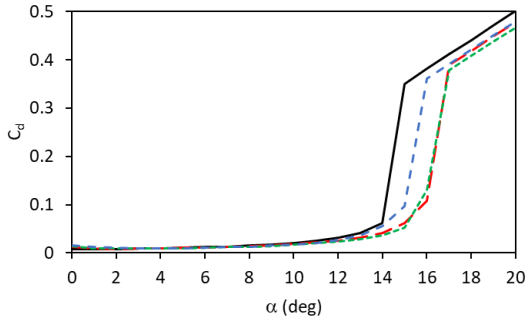

(a) $h_c = 0.05$

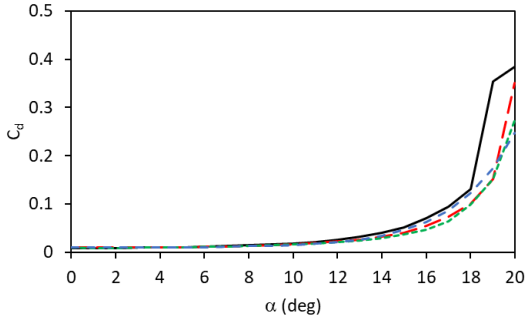

(b) $h_c = 0.3$

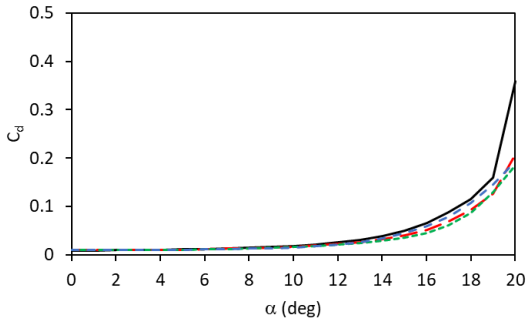

(c) $h_c = 0.4$

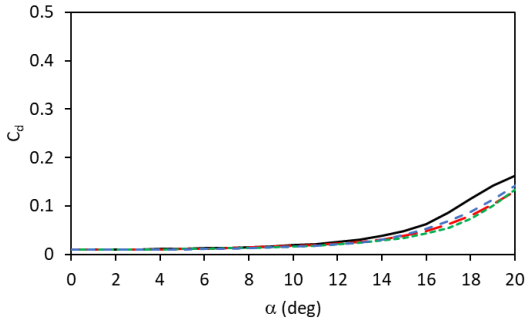

(d) $h_c = 1$

Fig. 17. Drag coefficient for different angles of attack.

This agreed with the published experimental and numerical data [32, 33] which indicated that the reflexed airfoil sacrifices about 12% of the maximum lift to obtain less movement of the center of pressure. The results also indicated that the ground effect diminishes for h_c values between 0.3 and 0.4, which agreed with the published data [10-15].

The drag coefficient of all airfoils increases sharply at high α and extremely low ground clearance ($h_c = 0.05$) due to the flow congestion in the narrow passage below the airfoil and the large separation zone on the upper surface.

C_d of the reflexed airfoil increases more smoothly with increased α compared to the others at moderate ground clearance (h_c = 0.3 and 0.4), since the divergent passage below the reflexed trailing edge reduces flow congestion. The angle at which sharp increasing of C_d occurred decreases from 19° to 16° with the h_c from 0.3 to 0.05 in the flat-bottom airfoils and decreases from 18° to 14° in NACA6409.

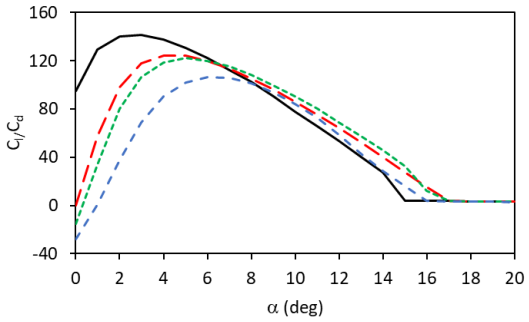

(a) h_c = 0.05

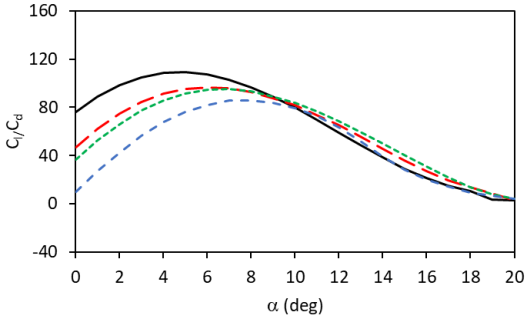

(b) h_c = 0.3

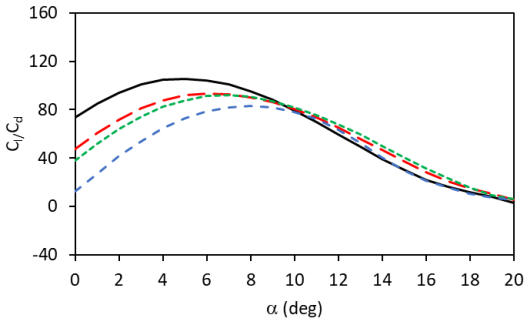

(c) h_c = 0.4

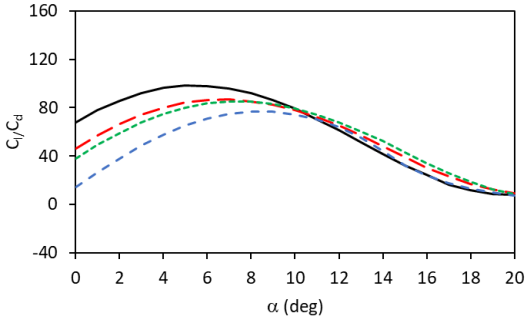

(d) h_c = 1

Fig. 18. Lift-to-Drag ratio for different angles of attack.

The lift-to-drag ratios for these four airfoils are shown in Fig. 18. At h_c of 0.05, NACA6409 has the highest ratio of 142 at 3°, followed by NACA4412 with the ratio of 124 at 4°, Clark-Y of 122 at 5° and N60R of 106 at 7°, respectively. However, a drastic decrease in lift-to-drag of NACA6409 occurs after its maximum. NACA4412 and Clark-Y lift-to-drag ratios are almost identical.

The comparison of the characteristics of the selected airfoils are summarized in the following tables.

Table 1. Characteristics of NACA6409, NACA4412, Clark-Y and N60R at h_c=0.05.

Airfoils	NACA 6409	NACA 4412	Clark-Y	N60R
C_l at stall	1.68 (14°)	1.68 (14°)	1.67 (15°)	1.56 (14°)
Min. C_d	0.0077 (1°)	0.0084 (2°)	0.0085 (2°)	0.0094 (3°)
Max. C_l/C_d	142 (3°)	124 (4°)	122 (5°)	106 (7°)
C_m at $(C_l/C_d)_{max.}$	-0.195	-0.141	-0.124	-0.065
X_{cp} at $(C_l/C_d)_{max.}$	41%c	37%c	36%c	30%c

Table 2. Characteristics of NACA6409, NACA4412, Clark-Y and N60R at h_c=0.3.

Airfoils	NACA 6409	NACA 4412	Clark-Y	N60R
C_l at stall	1.53 (14°)	1.48 (14°)	1.47 (15°)	1.35 (13°)
Min. C_d	0.0087 (0°)	0.0092 (1°)	0.0090 (1°)	0.0093 (2°)
Max. C_l/C_d	109 (5°)	97 (6°)	95 (7°)	86 (8°)
C_m at $(C_l/C_d)_{max.}$	-0.142	-0.100	-0.082	-0.023
X_{cp} at $(C_l/C_d)_{max.}$	37%c	34%c	32%c	27%c

Table 3. Characteristics of NACA6409, NACA4412, Clark-Y and N60R at h_c=1.0.

Airfoils	NACA 6409	NACA 4412	Clark-Y	N60R
C_l at stall	1.58 (13°)	1.51 (14°)	1.48 (15°)	1.34 (13°)
Min. C_d	0.0094 (0°)	0.0099 (0°)	0.0094 (0°)	0.0094 (1°)
Max. C_l/C_d	98 (5°)	87 (7°)	85 (7°)	77 (8°)
C_m at $(C_l/C_d)_{max.}$	-0.134	-0.087	-0.069	-0.048
X_{cp} at $(C_l/C_d)_{max.}$	37%c	33%c	32%c	26%c

4. Conclusion

A comparative study of four airfoils, NACA6409, NACA4412, Clark-Y and N60R in ground effect was conducted by investigating aerodynamic characteristics based on the computational results at Re of 3×10^6 and the ground clearance from 5% to 100% of the chord. For all selected airfoils, the effects of the ground on C_l, C_d, C_m and X_{cp} become significant when the ground clearance (h_c) is less than 0.4.

NACA6409 has the highest lift before stall. The stall occurs at lower α compared with the others, especially at low ground clearance. The minimum drag of NACA6409 is also the lowest, which results in the highest lift-to-drag ratio among these four airfoils. However, it has a greater movement of the center of pressure and a strong nose-down moment. This requires greater control power and a larger tail plane area to maintain pitch stability, in contrast to N60R which has smallest maximum lift and the highest minimum drag account for the lowest lift-to-drag ratio because of the reflexed trailing edge. Even if it requires a larger wing surface, it has a lower movement of the center of pressure, resulting in a smaller change in pitch stability. The pitching moment coefficient is almost zero over the useful length of α (2-15°) for the reflexed airfoil, but the nose-down moment increases when $h_c < 0.4$. The maximum lift-to-drag ratio is achieved at α around 6 to 7°. Clark-Y has slightly better performance than NACA4412 and the performance of both flat-bottom airfoils lie between NACA6409 and N60R.

Acknowledgement

The author would like to thank Graham K. Rogers, English Language Adviser, Faculty of Engineering, Mahidol University, for constructive criticism of the manuscript, and CAD-FEM SEA Pte. Ltd. – a certified Elite Channel Partner to ANSYS – for providing support and access to the CFD program named ANSYS Fluent 2021 R1.

References

[1] International Maritime Organization, "Guidelines for wing-in-ground craft," IMO, London, MSC.1/Circ.1592, 2018.

[2] M. S. Selig, J. F. Donovan, and D. B. Frase, *Airfoils at Low Speeds*. Virginia: H.A. Stokely, 1989.

[3] K. H. Jung, H. H. Chun, H. J. Kim, "Experimental investigation of wing-in-ground effect with a NACA6409 Section," *J. Mar. Sci. Technol.*, vol. 13, no. 4, pp. 317-327, 2008.

[4] M. Tahani, M. Masdari, and A. Bargestan, "Aerodynamic performance improvement of WIG aircraft," *Aircr. Eng. Aerosp. Technol.*, vol. 89, pp. 120-132, 2017.

[5] S. Jamei, A. Maimun, N. Azwadi, M. M. Tofa, S. Mansor, and A. Priyanto, "Static stability and ground viscous effect of a compound wing configuration with respect to Reynolds number," *Adv. Mech. Eng.*, vol. 6, 2015.

[6] R. Ranzenbach and J. Barlow, "Cambered airfoil in ground effect—An experimental and computational study," *SAE Technical Paper*. 1996.

[7] C. M. Hsiun and C. K. Chen, "Aerodynamic characteristics of a two-dimensional airfoil with ground effect," *J. Aircr.*, vol. 33, no. 2, 1996.

[8] A. Firooz and M. Gadami, "Turbulence flow for NACA 4412 in unbounded flow and ground effect with different turbulence models and two ground conditions: Fixed and moving ground conditions," *Korea Soc. Comput. Fluids Eng.*, pp. 49-50, 2006.

[9] M. R. Ahmed and T. Takasaki, Y. Kohama, "Aerodynamics of a NACA4412 airfoil in ground effect," *AIAA J.*, vol. 45, no. 1, 2007.

[10] A. E. Ockfen and K. I. Matveev, "Aerodynamic characteristics of NACA 4412 airfoil section with flap in extreme ground effect," *Int. J. Nav. Archit. Ocean Eng.*, vol. 1, no. 1, 2009.

[11] S. Y. Win and M. Thianwiboon, "Parametric Optimization of NACA 4412 Airfoil in Ground Effect Using Full Factorial Design of Experiment," *Eng. J.*, vol. 25, no. 12, pp. 9-19, 2021.

[12] W. Yang and Z. Yang, "Effects of design parameters on longitudinal static stability for WIG craft," *Int. J. Aerodyn.*, vol. 1, no. 1, 2010.

[13] S. Y. Shin, K. H. Whang, K. S. Kim, and J. H. Kwon, "Evaluation of longitudinal stability characteristics based on Irodov's criteria for wing-in-ground effect," *Trans Jpn Soc. Aeronaut. Space Sci.*, vol. 53, no. 182, pp. 237-242, 2011.

[14] Q. Jia, W. Yang, and Z. Yang, "Numerical study on aerodynamics of banked wing in ground effect," *Int. J. Nav. Archit. Ocean Eng.*, vol. 8, no. 2, 2016.

[15] H. H. Chun and C. H. Chang, "Turbulence flow simulation for wings in ground effect with two ground conditions: fixed and moving ground," *Int. J. Marit. Eng.*, vol. 145, no. A3, pp.1-18, 2003.

[16] F. H. Bramwell, "Further experiments with airfoils having reversed curvature towards the trailing edge," *British A.C.A. R. and M.*, vol. 110, no. 3, 1914.

[17] K. V. Rozhdestvensky, "Wing-in-ground effect vehicles," *Prog. Aerosp. Sci.*, vol. 42, no. 3, 2006.

[18] R. M. Pinkerton, "The variation with Reynolds number of pressure distribution over an airfoil section," Langley Memorial Aeronautical Laboratory, NACA-TR-613, 1938.

[19] M. Halloran and S. O'Meara, "Wing in ground effect craft review," The Sir Lawrence Wackett Centre for Aerospace Design Technology, Royal Melbourne Institute of Technology, Melbourne, Australia, 1999.

[20] F. R. Menter, "Two-equation eddy-viscosity turbulence models for engineering applications," *AIAA J.*, vol. 32, no. 8, 1994.

[21] "Turbulence," in *ANSYS Fluent Theory Guide, Release 2021 R1*. Canonsburg, PA: ANSYS, Inc., 2021.

[22] M. M. Munk and E. W. Miller, "The variable density wind tunnel of the National Advisory Committee for

Aeronautics," Langley Memorial Aeronautical Laboratory, NACA-TR-227, 1926.
[23] E. N. Jacobs, K. E. Ward, and R. M. Pinkerton, "The characteristics of 78 related airfoil sections from tests in the variable-density wind tunnel," Langley Memorial Aeronautical Laboratory, NACA-TR-460, 1933.
[24] I. H. Abbott and A. E. Doenhoff, "Summary of airfoil data," Langley Memorial Aeronautical Laboratory, NACA-TR-824, 1945.
[25] Q. Qu, W. Wang, and P. Liu, "Airfoil aerodynamics in ground effect for wide range of angles of attack," *AIAA J.*, vol. 53, no. 4, 2015.
[26] M. Hepperle, *JavaFoil*. Accessed: 1 April 2020. [Online]. Available: https://www.mh-aerotools.de/airfoils/
[27] R. Eppler, "Praktische Berechnung laminarer und turbulenter Absauge-Grenzschichten," *Ing.-Archiv.*, vol.32, no. 4, pp. 221-245, 1963.
[28] R. Eppler, "Turbulent Airfoils for General Aviation," *J. Aircr.*, vol.15, no. 2, pp. 93-99, 1978.
[29] R. Eppler and D. M. Somers, "A computer program for the design and analysis of low-speed airfoils," NASA Langley Research Center, Hampton, VA, United States, NACA-TM-80210, L-12937, 1980.
[30] T. Chitsomboon and C. Thamthae, "Adjustment of k-ω SST turbulence model for an improved prediction of stalls on wind turbine blades," in *Proc. World Renew. Ener. Congr.*, 2011, pp. 4114 – 4120.
[31] R. D. Irodov, "Criteria of the longitudinal stability of the ekranoplan," Defense Technical Information Center, 1974.
[32] G. L. Defoe, "A comparison of the aerodynamic characteristics of three normal and three reflexed airfoils in the variable density wind tunnel," Langley Memorial Aeronautical Laboratory, NACA-TN-388, 1931.
[33] M. Thianwiboon, "Numerical aerodynamic analysis of a reflexed airfoil, N60R, in ground effect with regression models," *IJTST.*, vol. 9, no. 1, 2021.

Mongkol Thianwiboon was born in Lampang, Thailand in 1976. He received the B.S. and M.S. and the Ph.D. degrees in mechanical engineering from Chulalongkorn University in 1997, 2000 and 2005 respectively.

From 2000 to 2005, he was a system administrator at Engineering Computer Center, Chulalongkorn University while studying the Ph.D. degree. After that, he worked with Lenso Wheel Co., Ltd as a project engineer during 2005 to 2008. Later, he was the manager of the Process Improvement Department during 2008 to 2011. Since 2011, he has been an faculty member of the Industrial Engineering Department, Mahidol University. His research interests include robotic and autonomous system and computational fluid dynamics. Dr. Thianwiboon is a member of the Council of engineers and Society of Automotive Engineers -Thailand (TSAE).